ELSEVIER

Solid State Ionics 143 (2001) 285–296

SOLID STATE IONICS

www.elsevier.com/locate/ssi

Ionic conductivity and pressure dependence of trigonal-to-cubic phase transition in lithium sodium sulphate

N. Bagdassarov [a], H.-C. Freiheit [b,*], A. Putnis [b]

[a] *Institut für Meteorologie und Geophysik, J. W. Goethe Universität-Frankfurt, Feldbergstraße 47, D-60323 Frankfort on the Main, Germany*

[b] *Westfälische Wilhelms-Universität, Institut für Mineralogie, Corrensstraße 24, D-48149 Münster, Germany*

Received 10 October 2000; received in revised form 30 January 2001; accepted 15 March 2001

Abstract

The pressure and temperature dependencies of electrical impedance as a function of frequency (from 0.1 Hz to 100 kHz) have been measured in crystalline $LiNaSO_4$ over temperature range 400–800°C and pressures 5, 10 and 20 kbar in a piston–cylinder apparatus. The cell for electrical impedance measurements represents a co-axial cylindrical capacitor with a geometric factor 5.5–7 cm. $LiNaSO_4$ undergoes a displacive first order phase transition from trigonal structure with a space group P31c to a body-centred cubic (bbc) structure with a high ionic conductivity > 0.1 S/cm (at 10 kHz). The bulk resistance has been estimated at each temperature from Argand plots. The temperature of the phase transition has been estimated from plots of $\log[\sigma T]$ vs. $1/T$. A drop of the electrical impedance indicates that the phase transition occurred at 5 kbar at 578°C (± 1), at 10 kbar at 641°C and at 20 kbar at 764°C. There is small hysteresis of phase transition temperature observed by cooling, the hysteresis disappears with the pressure increase. The slope dT/dP estimated from the electrical conductivity measurements of this phase transition is 12.5°C/kbar and corresponds to Clausius–Clayperon slope with $\Delta S \sim 26.4$ J/mol/K and $\Delta V \sim 3.3$ cm^3/mol. In the extrinsic region, the electrical conductivity has an activation energy which varies from 1.48 eV at 5 kbar to 1.35 eV at 20 kbar, in the intrinsic region, the activation energy (E_a) is ca. 2.4–2.30 eV. In the high temperature conductive phase, E_a is ca. 0.33–0.4 eV, and does not depend on pressure. With the pressure increase, temperature intervals of extrinsic and intrinsic conductivities start to overlap, which results in a non-Arrhenian temperature dependence. The frequency dependence of the electrical conductivity at low frequencies (< 500 Hz) may be approximated as $\sigma \approx \sigma_0(1 + (j\omega\tau_0)^n)$, where ω is frequency, τ_0 is a temperature-dependent constant, and n is an experimental exponent characterising a low frequency dispersion (LFD). With the temperature increase from extrinsic region to fast ionic phase, n increases from 0 to ~ 0.5.

Keywords: $LiNaSO_4$; Ionic conductivity; Phase transition; High pressure

1. Introduction

The phase transition in $LiNaSO_4$ from trigonal to body-centred cubic (bcc) phase has been the focus of many experimental investigations [1]. The interest in electrical properties of $LiNaSO_4$ is due to a possible

* Corresponding author. Present address: Wacker Chemie GmbH, Werk Burghausen, D-84480 Burghausen, Germany. Tel.: +49-8677-83-8349; fax: +49-8677-83-5497.

E-mail addresses: nickbagd@gephysik.uni-frankfurt.de (N. Bagdassarov), hans-christof.freiheit@wacker.com (H.-C. Freiheit).

0167-2738/01/$ - see front matter
PII: S0167-2738(01)00849-9

use of this material in solid-state batteries. A high temperature Li-battery must have a good ionic conductivity at operating (>650 K) temperatures and negligible conductivity at storage (from 230 to 340 K) temperatures [2]. At normal pressure, the transition to high temperature bcc phase of $LiNaSO_4$ takes place at 788 K and has a latent heat of 20.8 kJ/$\cdot$ mol, which is much larger than the heat of melting of 4.1 kJ/mol [3]. The thermal conductivity in the related compound Li_2SO_4 exhibits a λ-like behaviour as a function of temperature, jumping from 3 to 15 W/mol/K at the phase transition [4]. At high temperature, $LiNaSO_4$ is a solid electrolyte possessing a DC-electrical conductivity of about 1 S/cm, ascribed to the high cation mobility. It has been pointed out in numerous publications (c.f. Refs. [1,5–10]) that strong rotational oscillations must be expected for sulphate groups at high temperatures, thus, lithium and sodium ions may move between tetrahedral and octahedral positions in high temperature bcc phase. Thus, the term 'paddle-wheel' or 'cog-wheel' mechanism has been introduced to describe this coupling between a rotational disorder of translationally immobile sulphate ions and an enhanced mobility of alkaline ions [7]. Raman-scattering studies of $LiNaSO_4$ in ν_4-spectral region (680–600 cm^{-1}) confirmed a breakdown of correlated coupling vibrations of sulphate ions within the unit cell [11]. As an alternative, it has been suggested that the superionic conducting properties of β-$LiNaSO_4$ phase may be attributed to a percolation threshold of cations in the more open bcc structure at high temperature [12–15]. Electrical conductivity measurements on $LiNaSO_4$ doped with guest ions WO_4^- supported the 'free volume' concept that the intersite mobility of alkali cations is due to a simple sublattice expansion.

Measurements of the magnetic nuclear relaxation on $LiNaSO_4$ revealed quadrupolar and dipolar relaxation of Li^+ and Na^+ ion defects [16] having activation energies 1.9_{Li} and 1.74_{Na} eV (dipole) 0.8_{Li} and 1.34_{Na} eV (quadropole), which are comparable to the activation energy for DC-electrical conductivity of 1.59 eV in the extrinsic region.

Recent results on molecular dynamic simulations [17] and reverse Monte Carlo modelling [8] indicated a more sophisticated process of cation migration. The enhanced mobility of Li and Na cations in sulphates may be caused by at least three processes: (1) contributions from lattice thermal vibrations; (2) contributions from centre-of-mass fluctuations of sulphate ions ('gate percolation'); (3) contributions from reorientation of sulphate anion complexes.

Experimental results on high temperature single crystal and powder diffraction [3] demonstrated a strong first order character of the phase transition trigonal-to-cubic structure of $LiNaSO_4$ and a λ-like increase of the specific heat. The transition represents some continuous and discontinuous changes in the structure with temperature. The continuous part includes a displacement of sulphur atoms and increasing of rotational disorder of sulphate ion complexes with the temperature increase. The discontinuous part associates with an onset of cationic 'sublattice melting'.

Only few experiments have been done to determine this phase transition under pressure. The *P–T*-phase diagram of Li_2SO_4 has been studied up to 800°C and 4 GPa by DTA [18] and electrical resistance measurements [19]. The *P–T*-diagram of Na_2SO_4 has been investigated up to 450°C and 4.5 GPa by DTA [20]. To the author's knowledge the pressure dependence of trigonal-to-cubic phase transition in $LiNaSO_4$ has not been reported yet. Recent Raman studies at room temperature suggest that $LiNaSO_4$ transforms to an orientationally disordered structure (pressure-induced amorphization) between 22 kbar [21] and 23.9 kbar [22].

The main purpose of this study is to characterise a pressure dependence of trigonal-to-cubic phase transition in $LiNaSO_4$ by the use of AC-conductivity measurements.

2. Experimental

In this study, we have used a conventional piston–cylinder apparatus to perform electrical conductivity measurements at pressures up to 20 kbar and temperatures up to 900°C. The press consists of two hydraulic cylinders: one is to perform an end-load and the second is to move a piston. The diameter of the high pressure autoclave is 1/2″ (Danfoss™, Denmark). The inner part of a high pressure cell is shown in Fig. 1. The pressure calibration of the cell has been done by the use of some standard point

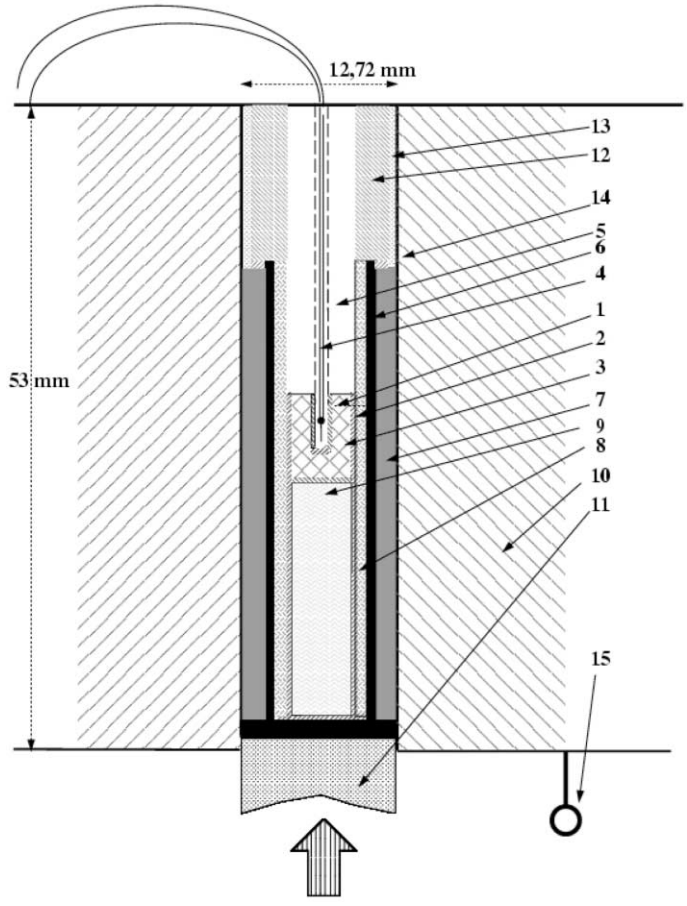

Fig. 1. Principal scheme of a piston–cylinder cell used for electrical impedance measurements: 1—inner cylindrical Pt-electrode; 2—outer cylindrical Pt-electrode; 3—sample; 4—thermocouple S-type; 5—Al_2O_3-ceramic Alsint-99,7; 6—graphite heater; 7—CaF_2 pressure transmitting medium; 8—boron nitride; 9—ceramic AlSiMag or boron nitride; 10—WC-hard metal core; 11—WC-hard metal piston; 12—plug of stainless steel; 13—unfired pyrophyllite; 14—copper-ring, 15—electrical contact-ground of the press.

materials: at room temperature, the transformations Bi I–II–III at 25.55 and 27.0 kbar [23] have been used; at high temperature, melting curves of NaCl and CsCl [24] have been used. Melting points of these substances as a function of pressure up to 25 kbar have been determined in-situ by electrical conductivity measurements. At a melting point, the observed drop in the electrical impedance at 1 kHz was ca. 2 orders of magnitude. The performed pressure calibration believed to be within an accuracy of ± 0.3 kbar. The temperature gradient in the cell has been estimated on dummy samples of pressed Al_2O_3 powder by the use of three thermocouples. The estimation for a radial temperature gradient is ca. 1°/mm, for a vertical temperature gradient, it is ca. 2°/mm in the temperature range up to 900°C.

Electrical impedance measurements have been done with Solartron 1260 Phase-Gain-Analyser interfaced with a PC. The device permits a single sine drive and analysis of a system under test over the frequency range 10 μHz to 32 MHz. In high pressure experiments, we applied 1 V sine signal in frequency range 0.01 Hz to 100 kHz.

A cell for electrical impedance measurements represents a coaxial cylindrical capacitor with a geometric factor 5–7 cm filled with a sample under test. The exact geometric factor of a cell has been evaluated independently from calibration measurements

on NaCl solutions (0.01–3 M) at 22°C and pressure 1 bar. For these purposes, a cylindrical gap between two Pt-electrodes (made of Pt-foil 0.05 mm in thickness) has been filled with a NaCl-solution of a known molar concentration. The measured conductivity of NaCl-solutions has been compared with the table values [25]. The difference between a calculated geometric factor of a cylindrical capacitor:

$$G = 2\pi \frac{L}{\ln\left(\frac{D}{d}\right)}, \quad (1)$$

and a measured geometric factor was about 25%, where D is the diameter of an outer electrode, d is the diameter of an inner electrode, L is the length of cylinders.

During impedance measurements, the press was separated from the ground of Solartron 1260. Wires of Pt-thermocouple and the mass of the high pressure autoclave were used to connect the measuring device and the cell electrodes. Before doing the high pressure experiments a measuring cell has been calibrated for short cut impedance and for an open circuit impedance in a frequency range 1 MHz–0.01 Hz. A typical AC-resistance of the cell to a short connection is 0.4 Ω. These calibrations have been taken into account in final calculations of the electrical impedance as a function of frequency. At high pressure and temperature, the measurements of the electrical impedance were conducted without an automatic temperature control in order to reduce electrical noise of the heater.

Samples of $LiNaSO_4$ were in the form of a crystalline powder prepared from melting equimolar proportions of Li_2SO_4 and Na_2SO_4 at 973 K. Powder samples were dried in a furnace at 423 K over 24 h, and then pressed into the cylindrical gap between two coaxial Pt-foils (Fig. 1). During the experiments, the upper and lower parts of the piston–cylinder bomb were cooled with running water, providing a temperature of ca. 450 K of piston, stainless steel plug and pyrophillite ring. At this temperature, the shunting effect of the unfired pyrofillite ring on a measured resistance of samples is negligible. Experiments were conducted at fixed pressures 5, 10 and 20 kbar with increasing and decreasing temperature. The AC-current ca. 150 A and 12 V was supplied to the graphite heater. The noise from 50 Hz harmonic was effectively suppressed by Solartron 1260, and an induction effect of 50 Hz harmonics was not observed on frequency scans. The geometry of a cell was inspected under an optical microscope before and after experiments. The measurable changes in geometric factor were as follows: $\Delta D < -0.5\%$, $\Delta d < +2\%$, $\Delta L < -4\%$. The total changes of the geometric factor were about 5%.

3. Results

At each temperature during heating and cooling cycles we have measured electrical impedance from a frequency scan 100 kHz–0.1 Hz. The data of imaginary $\mathrm{Im}(Z)$ and real $\mathrm{Re}(Z)$ components of impedance were plotted on a Argand-graph. The bulk AC-conductivity has been estimated from Argand-plot as point of intersection of $\mathrm{Im}(Z)$ with the horizontal axis (Fig. 2). Usually, this point corresponds to a frequency range from 15 (at low temperatures corresponding to β-phase) to 60 kHz (at high temperatures corresponding to α-phase). The observed bulk AC-conductivity in the α-phase is ca. 10^{-1} S/cm, e.g. nine times smaller than the value at 823 K reported from DC-measurements at 1 bar by using U-cell (c.f. Ref. [1]). On the other hand, this conductivity fits well with the results of other high frequency measurements 0.12 S/cm at 788 K and 1 MHz [16], but it is higher than the result 0.02 S/cm at 800 K and 1 Hz–10 kHz obtained by Gundusharma et al. [13].

This difference may be due to several reasons: (1) We have estimated the AC-bulk conductivity for the high frequency range. The conductivity obtained from impedance spectroscopy measurements is usually less than from DC-measurements. For example, in the system $LiNaSO_4$:LiCl (in the proportion of 9:1), the AC-conductivity at 798 K is 0.6 S/cm at 1 kHZ and DC-conductivity is 1.1 S/cm [26]. (2) The geometric factor of the cell was 5–7 cm. This means that the measured bulk resistance of a sample having a conductivity 0.1 S/cm is about 1.4 Ω. This may be too close to the minimum resolvable electrical impedance in the experiments which we estimate ca. 0.5 Ω. Contrary to some complex impedance plots reported

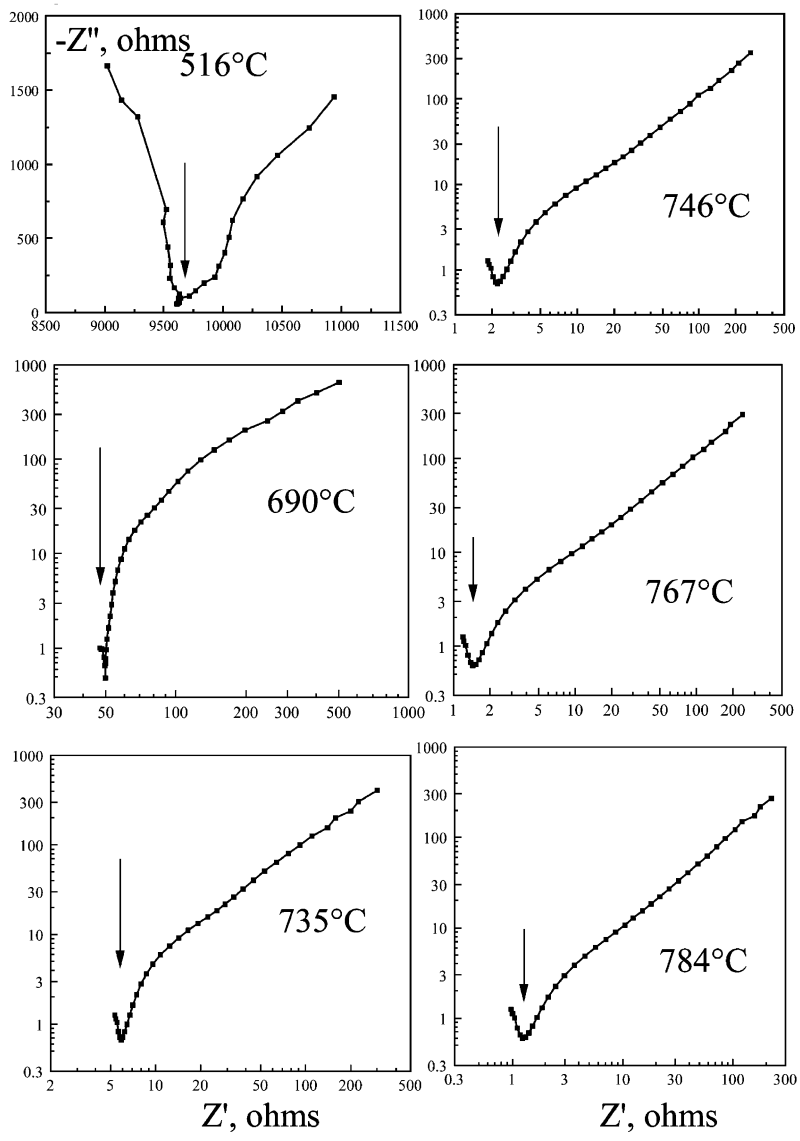

Fig. 2. Argand diagram for $LiNaSO_4$ at 20 kbar. At each temperature, the bulk resistance (marked by arrows) has been estimated from frequency scan of electrical impedance as a value of Z' (Ω), corresponding to a minimum value of $-Z''$ (Ω). Frequency increases from right to left.

by Prabaharan et al. [26], we could resolve a minimum in Argand-plots even at temperatures where the α-phase is stable. Basically, the electrical impedance scans in this study mimics the plots obtained by Kanashiro et al. [16] from AC-conductivity measurements.

The data of AC-conductivity measurements at 5, 10 and 20 kbar are presented in Fig. 3. The scatter of the impedance measurements $|Z|$ reflects small difference in the geometric factor of different runs. The data of AC-conductivity, which are presented as $\log[\sigma T]$, are less scattered. From the graph, the

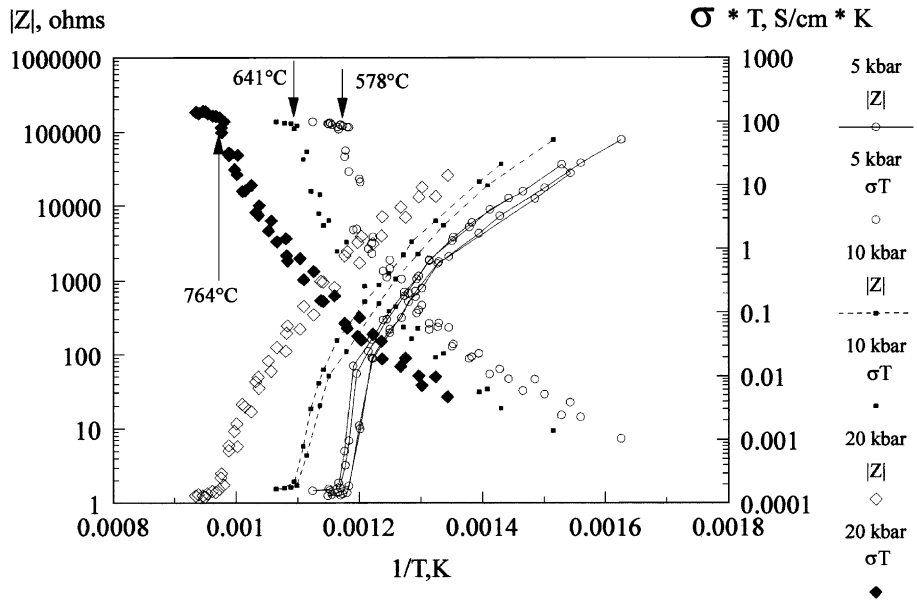

Fig. 3. Bulk-electrical impedance and electrical conductivity of $LiNaSO_4$ for 5, 10 and 20 kbar. Arrows indicate the phase transformation temperature. There is small hysteresis in the phase transition temperature, which disappears with the pressure increase.

point of a phase transition may be estimated as temperature at which there is a kink in a slope of $\log[\sigma T]$ as function of $1/T$.

Fig. 4 presents a pressure dependence of the phase transition temperature. The slope of dT/dP is about 12.5 K/kbar, which corresponds to a CC slope calculated from $\Delta V = 3.3$ cm^3/mol and $\Delta S = 26.4$ J/mol/K of this phase transition at 1 bar [3].

Traditionally, the ionic conductivity is regarded as a product of three factors: mobility, charge and density of charge carriers. For the analysis below we have fitted the AC-conductivity data at different temperature intervals to the Arrhenius-type expression:

$$\sigma T = \left(\frac{Ne^2\lambda^2\nu\gamma}{k}\right)\exp\left(-\frac{E_a}{kT}\right), \quad (2)$$

where e is ionic charge, λ is a distance between two jumps, γ is a geometry factor, N is a number of ions in a volume unit, ν is a jump frequency, k is the Boltzmann constant, E_a is the apparent activation energy for ionic motion. The results of fitting are summarised in Table 1.

The temperature dependence of $\log[\sigma T]$ as a function of $1/T$ has a kink at temperature T^* below the transformation temperature. In the temperature region below T^*, impurities or vacancies are fixed (n does not depend on temperature), and they control the defect concentration and the activation energy of the electrical conductivity (extrinsic region):

$$E_a = \Delta h_m, \quad (3)$$

where Δh_m is an activation energy of vacancy migration (e.g. Ref. [27]). At temperatures above T^*, the number of vacancies is also changed with temperature because of the thermal activation of defects, and thus, the activation energy of electrical conductivity is:

$$E_a = \Delta h_m + \Delta h_f/2, \quad (4)$$

where Δh_f is the activation energy of the vacancy formation. Results in Table 1 demonstrate that with pressure the activation energy of the vacancy formation remains constant 1.8–1.84 eV. The activation energies of extrinsic and intrinsic DC-measurements at 1 bar are 2.23 and 1.59 eV, respectively [16]. This provides an activation energy of defect formation of 1.28 eV. The activation energy of the electrical conductivity in the high temperature phase does not depend on pressure. The value of E_a of electrical conductivity in α-phase is ca. 0.35 eV, which is

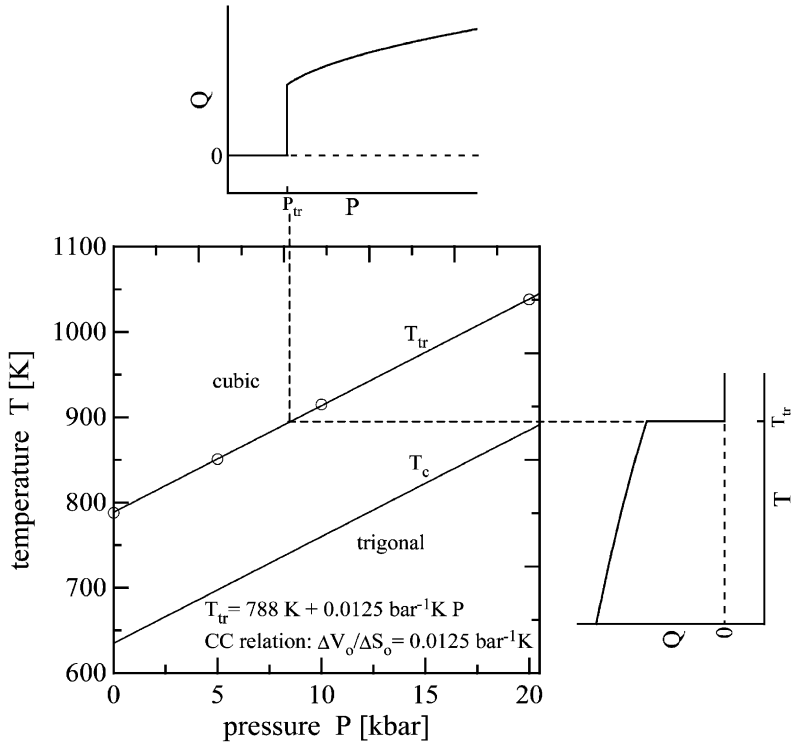

Fig. 4. Phase diagram of $LiNaSO_4$. Estimates of the p, T dependence of the trigonal-to-cubic phase transition at T_{tr} from bulk resistivity data. The critical temperature T_c is given by Eq. (13a). Both lines correspond to a CC slope of 0.0125 bar^{-1} K calculated from $\Delta S_0 = 26.4$ J/mol/K and $\Delta V_0 = 3.3$ cm^3/mol. The order parameter behaviour for a temperature- (right) and pressure (above)-induced phase transition are also shown.

slightly less than 0.44 eV [6], and the result measured from DC-measurement at 1 bar and about the same as has been reported from AC-measurements 0.32 eV [13]. Non-measurable small value of the activation volume in $LiNaSO_4$, i.e. pressure-independent activation energy of the electrical conductivity

Table 1
Activation energies of electrical conductivity of $LiNaSO_4$ in α- and β-phases

$E_a(\sigma,T)$, eV	5 kbar	10 kbar	20 kbar
T^*, transition temperature of extrinsic–intrinsic conductivities	490°C	520°C	620°C
β-phase ($T \ll T_{tr}$)	1.48 ± 0.07	1.45 ± 0.06	1.35 ± 0.08
Extrinsic conductivity:	(T < 490°C)	(T < 520°C)	(T < 620°C)
Concentration of vacancies = const			
β-phase ($T < T_{tr}$)	2.40 ± 0.08	2.35 ± 0.05	2.27 ± 0.07
Intrinsic conductivity:	(490°C < T < 550°C)	(520°C < T < 600°C)	(700°C < T < 620°C)
vacancies are thermally activated			
α-phase ($T > T_{tr}$)	0.34 ± 0.05	0.35 ± 0.06	0.35 ± 0.05
	(565°C < T)	(640°C < T)	(765°C < T)
Δh_f, energy of crystal defect formation eV	1.84	1.80	1.84

σT (see Table 1), compares with low activation volume in high temperature conductive f.c.c. phase of $Li_2SO_4 \sim 0.5$ cm^3/mol, in comparison with high temperature hexagonal phase of $Na_2SO_4 \approx 4.4$ cm^3/mol [28]. It may be also that the pressure range in experiments was not enough to impact significantly Li conduction through volume restriction [29].

Frequency dependence of electrical impedance in $LiNaSO_4$ at temperatures below and above the phase transition is shown in Fig. 5a–c.

The log–log form of electrical conductivity corresponds to the sum of two power-law functions of frequency:

$$\sigma(\omega) = \sigma_0(1 + (j\omega\tau_0)^n + \sigma_{AC}(1 + (j\omega\tau_{AC})^p). \quad (5a)$$

On a double logarithmic scale, the electrical conductivity in the low frequency range (< 200 Hz) can

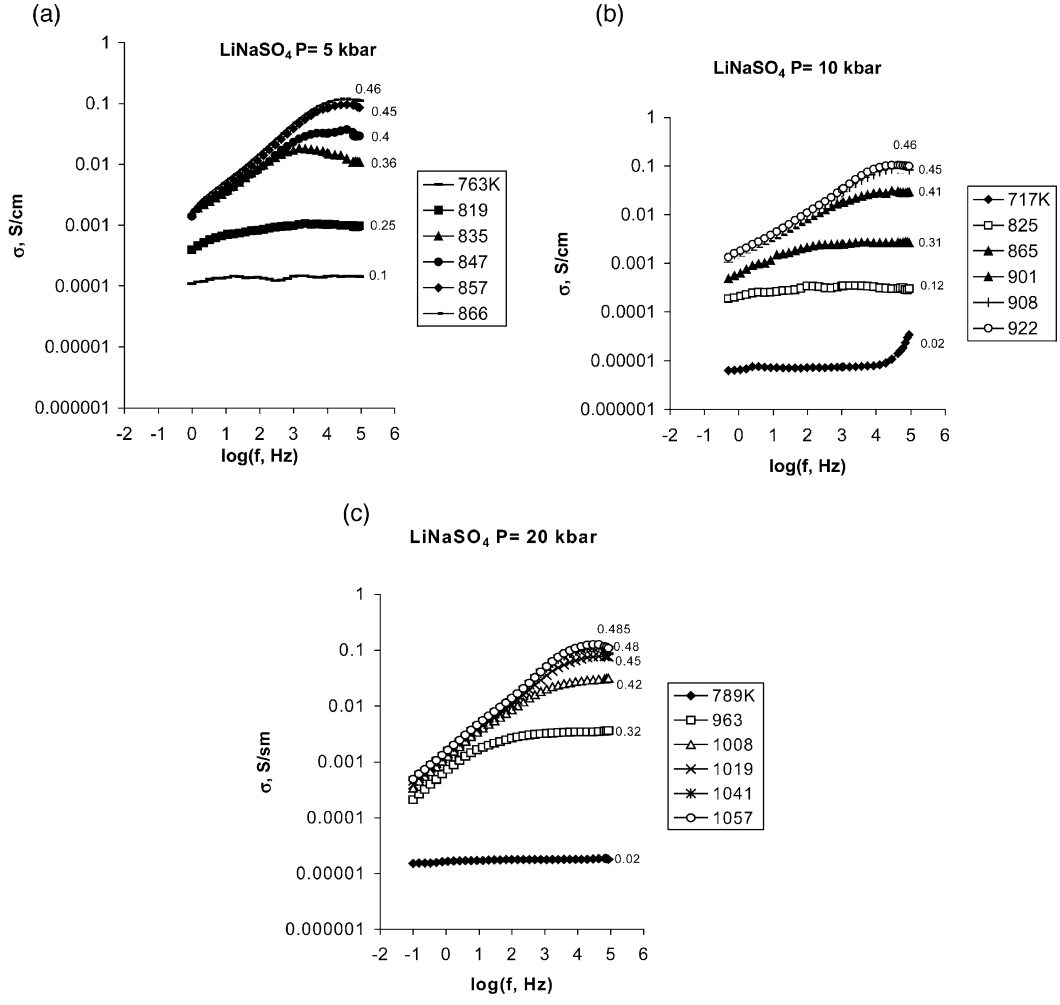

Fig. 5. (a) Electrical conductivity of $LiNaSO_4$ at 5 kbar as a function of frequency. Numbers at curves are exponent n in the fitting expression $\sigma \approx \sigma_0 + \text{const}\,\omega^n$ at low frequencies. (b) Electrical conductivity of $LiNaSO_4$ at 10 kbar as a function of frequency. (c) Electrical conductivity of $LiNaSO_4$ at 20 kbar as a function of frequency.

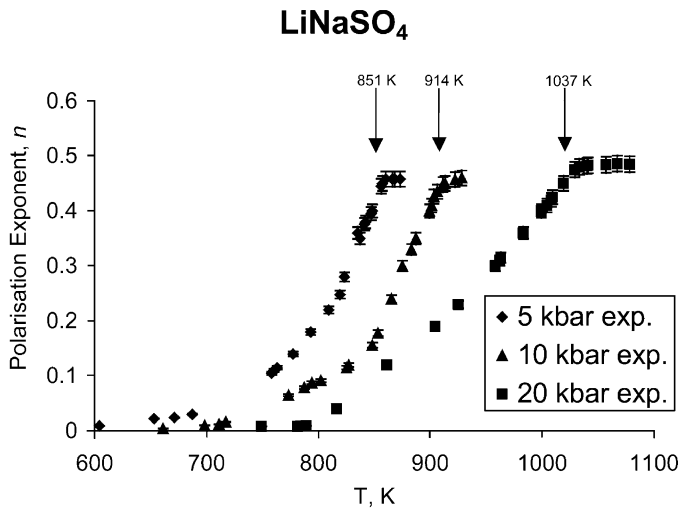

Fig. 6. Temperature dependence of the polarisation exponent for different pressure.

be approximated as a straight line indicating the relationship:

$$\sigma \sim \text{const}\,\omega^{n}, \tag{5b}$$

where ω is the frequency, τ_0 and τ_{AC} are temperature-dependent RC parameters of equivalent circuit at low- and high-frequencies, n is the low frequency dispersion exponent (LFD), which characterises the degree of electrical contact polarisation, p is the high frequency exponent, which characterises the sample polarisation, σ_0 and σ_{AC} are 'fictive' DC- and 'true' AC-conductivities, respectively (e.g. Refs. [30,31]). When $n \approx 0$, the substance is not electrically polarised near electrode–sample interface. A strong LFD, when $n \sim 1$, implies a finite and reversible storage of charge in the sample or at the interface [31]. Some authors relate LFD-exponent to the sample-electrode interface roughness, when the electrode–sample interface may be considered as a constant phase element [32].

By fitting the conductivity data at temperatures below and above the phase transition to Eq. (5a), we may estimate the degree of contact and sample polarisations, and bulk AC-conductivity of $LiNaSO_4$. The sample polarisation exponent p was about 1 and did not change across the phase transition. Contrary to sample polarisation, there is a noticeable variation of LFD-exponent p. At temperatures below the phase transition in the field of trigonal phase stability $LiNaSO_4$, the contact between sample and electrodes is not polarised ($n \approx 0$). In the vicinity of the phase transition temperature, the exponent n tends to 0.5. At temperatures in the field stability of cubic phase, the polarisation exponent remains constant at $n \approx 0.5$. The behaviour of the polarisation exponent at 5, 10 and 20 kbar as a function of temperature is shown in Fig. 6.

4. Pressure effect on polarisation and order parameter

Assuming that the degree of sample polarisation displays the rotation of the sulphate groups, its value should be correlated to the order parameter of the phase transition. Without reference to the specific nature of the orientational correlation functions (which include coupled librational motion of the sulphate groups, e.g. Ref. [33]), the order parameter behaviour can be deduced on macroscopical scale from lattice relaxation (spontaneous strain) that occurs as a secondary response to the cooperative changes on microscopic scale.

The general expression of the excess Gibbs free energy of a crystal with interacting order parameter Q and strain e has the form [34]:

$$G(Q,e) = L(Q) + G_{\text{coupling}}(Q,e) + G_{\text{elastic}}(e), \tag{6}$$

where $L(Q)$ is the standard Landau expansion of Q, G_{coupling} is the interaction energy between Q and e and G_{elastic} is the elastic energy from the relaxation of the unit cell. It is important to note that the Gibbs free energy in the above form accounts only for the intrinsic structural changes associated with the phase transition. At a pressure of 1 bar, the phase transition in $LiNaSO_4$ is strongly first order with e and Q linear-quadratically coupled ($e \propto Q^2$, improper ferroelastic). The Gibbs free energy can be written as [3]:

$$\begin{aligned}\Delta G(Q,e_i) = {} & \frac{1}{2}a(T-T_c)Q^2 + \frac{1}{4}BQ^4 \\ & + \frac{1}{6}cQ^6 + \lambda_t e_t Q^2 + \lambda_a e_a Q^2 \\ & + \frac{1}{2}C_t^0 e_t^2 + \frac{1}{2}C_a^0 e_a^2.\end{aligned} \tag{7}$$

Here T_c is the critical temperature, a, B and c are the normal Landau coefficients, e_t and e_a are the trigonal shear strain and the volume strain, λ_i are the strain/order parameter coupling coefficients and C_i^0 are the symmetry-adapted forms of the bare elastic constants (i.e. for the cubic phase). The thermodynamic character of the phase transition is determined by the value of B which is positive for a second order transition, negative for a first order transition and zero for a tricritical transition. In its renormalised form (i.e. $\partial G/\| e_i = 0$ for a stress-free crystal), the above equation becomes:

$$G(Q) = \frac{1}{2}a(T-T_c)Q^2 + \frac{1}{4}B^*Q^4 + \frac{1}{6}cQ^6, \tag{8}$$

where

$$B^* = B - 2\left(\frac{\lambda_t^2}{C_t^0} + \frac{\lambda_a^2}{C_a^0}\right) < 0. \tag{9}$$

The Landau coefficients have been estimated from fitting shear strain [3]: $T_c = 656$ K, $a = 0.112$ kJ/mol/K, $B^* = -124.8$ kJ/mol and $c = 198.1$ kJ/mol. It appears that the phase transition in $LiNaSO_4$ is not induced by strain-order parameter coupling since the strain renormalization does not lead to a positive value of the pure fourth order coefficient [35].

In the low temperature phase, the general behaviour of the order parameter is given by the well-known expression [34]:

$$Q = Q_0\sqrt{\frac{2}{3}\left[1 + \sqrt{1 - \frac{3}{4}\left(\frac{T-T_c}{T_{tr}-T_c}\right)}\right]}. \tag{10}$$

At the phase transition, the order parameter jumps from $Q = Q_0$ to $Q = 0$ in the paraphase:

$$Q_0 = \pm\left[\frac{-4a(T_{tr}-T_c)}{B^*}\right]^{1/2}. \tag{11}$$

Pressure dependence of the Gibbs free energy can be introduced by a term of the form $P\Delta V$, noting that the excess volume normally varies as $\Delta V \propto Q^2$. Thus, an additional quadratic term in Q has to be considered in the Landau expansion:

$$\begin{aligned}G(Q) = {} & \frac{1}{2}a(T-T_c)Q^2 + \frac{1}{4}B^*Q^4 + \frac{1}{6}cQ^6 \\ & + \frac{1}{2}a_v PQ^2,\end{aligned} \tag{12}$$

where a_v is a pressure coefficient that has the same sign as the excess volume. Subsequently, this leads to a renormalization of the critical temperature as well as the transformation temperature:

$$T_{tr} = T_c + (3B^{*2}/16ac), \tag{13a}$$

$$T_c^* = T_c - \frac{a_v}{a}P. \tag{13b}$$

The excess entropy and the excess volume at the phase transition are given by the harmonic parts of the free energy:

$$\Delta S_0 = -\left(\frac{\partial G}{\partial T}\right)_p = -\frac{1}{2}aQ_0^2, \tag{14a}$$

$$\Delta V_0 = \left(\frac{\partial G}{\partial p}\right)_T = \frac{1}{2}a_v Q_0^2, \tag{14b}$$

which are related through the classical CC rule with the slope of the equilibrium line in the phase diagram:

$$\frac{dT}{dp} = \frac{\Delta V_0}{\Delta S_0} = -\frac{a_v}{a}. \quad (15)$$

In agreement with the experimental data, the shift of the transition temperature by applied hydrostatic pressure strictly follows the CC slope (Fig. 4), and hence $a_v = -1.4$ J/mol/bar.

Fig. 7 shows the temperature evolution of the order parameter for different pressures calculated from Eq. (10) considering the change of T_c and T_{tr}. As was to be expected, the value of Q^2 increases with increasing pressure (stabilization of the trigonal phase at high pressure). It has to be emphasized that in this approach, the size of the discontinuity Q_0 remains invariable. However, the electrical conductivity as well as the polarisation coefficient (Fig. 6) suggest a decrease of the first order character when the pressure is increased. This behaviour may indicate that higher order coupling of the form $\Delta V = \alpha Q^2 + \beta Q^4$ becomes significant on increasing pressure which gives rise to a pressure renormalization of the fourth order term. The effect of this is to decrease the size of the first order step, i.e B^* increases. We recall that this does not necessarily mean a violation of the CC rule, when ΔV and ΔS are expected to change at the same rate. On the other hand, we have to consider that a change of pressure always produces an extrinsic volume change. This demonstrates the general limits of the validity of Landau theory when pressure dependence is incorporated. The model assumes that any volume change that is not associated with the phase transition is negligible. Hence, it is very likely that with increasing pressure, the values of the higher order Landau coefficients itself will change significantly [36]. It has to be noted that the Landau free energy is an expansion of the free energy in the vicinity of the phase transition, where the higher order terms vary slowly than the quadratic term. Whilst further structural and calorimetric investigations at high pressure and temperature are still needed, an empirical modification of the pressure dependence seems to be rather unsuitable to obtain a self-consistent picture of the phase diagram.

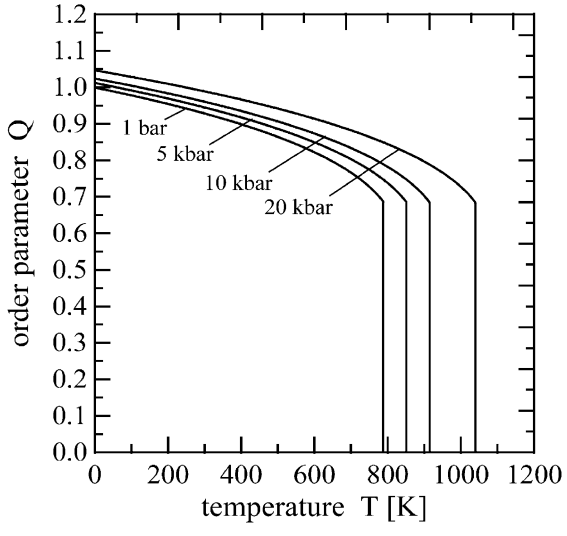

Fig. 7. Order parameter vs. temperature for different pressures based upon second order pressure renormalization. The order parameter is scaled to give $Q = 1$ at $T = 0$ K and $p = 1$ bar.

5. Conclusions

(1) The measured values of electrical conductivity of ionic conduction of bcc phase $LiNaSO_4$ at high pressures 0.1 S/cm (10 kHz) are higher than the results 0.02 S/cm at 800 K and $1–10^4$ Hz, reported by Gundusharma et al. [13], and close to 0.15 S/cm (800 K and 1 MHz) obtained by Kanashiro et al. [16]. The bulk AC-conductivity obtained from Argand (or Cole–Cole) plots in this study is smaller than the conductivity of $LiNaSO_4$ from DC-measurements 0.93 S/cm at 823 K [6] or 0.8 S/cm [26]. The measured value of the activation energy of ionic conduction 0.35 eV is closer to the data of the Antigonish group 0.37 ± 0.03 eV [13] rather than to the results of Gothenburg group 0.44 eV [5].

(2) The experimental data obtained for the electrical conductivity of $LiNaSO_4$ at three different pressures 5, 10 and 20 kbar indicate a pressure-independent activation energy for ionic conduction E_a and activation energy of vacancy formation Δh_f in the high temperature phase (HP). This means that the activation volume of conduction in HP of $LiNaSO_4$ is about zero. In general, the activation volume is

correlated with a degree of the volume change required for a cation (Li, Na) 'percolation' through SO_4 anion network. If activation volume is small, this implies that the 'percolation' process of cations contribute less to the conduction mechanism in HP of $LiNaSO_4$ than other mechanisms (e.g. rotation of SO_4-groups).

(3) The temperature dependence of the LFD exponent n may be correlated with the degree of rotational disorder of SO_4-anion complexes near the contact interface. However, the continuous behaviour of n vs. temperature appears to be incompatible with the first order character of the transition observed at 1 bar. One may thus speculate that the phase transition changes its character with increasing pressure *or* that n may be associated not only with changes of the long range order parameter (Q) but also of some short range order parameter.

Acknowledgements

This work is supported by a grant from the Deutsche Forschungsgemeinschaft (SFB 458). The authors are grateful to R. Secco and E. Secco for the comments on the early version of the manuscript, and to R. Tärneberg, A. Lundén for the reprints of their papers.

References

[1] A. Lundén, Solid State Commun. 65 (1988) 1237.
[2] A.D. Robertson, A.R. West, A.G. Ritchie, Solid State Ionics 104 (1997) 1.
[3] H.-C. Freiheit, H. Kroll, A. Putnis, Z. Kristallogr. 213 (1998) 575.
[4] A. Lundén, B.M. Suleiman, E. Karawacki, Heat transfer in the system Li_2SO_4–Na_2SO_4 in the range 300–900 K. in: H.A. Øye, O. Wærnes (Eds.), The International Terje Østvold Symposium in Røros—Norway. Norway Inst. Techn., Trondheim, 1998, pp. 65–75.
[5] A. Lundén, J. Solid State Chem. 107 (1993) 296.
[6] A. Lundén, Solid State Ionics 68 (1994) 77.
[7] A. Lundén, Z. Naturforsch. 50a (1995) 1067.
[8] L. Karlsson, R.L. McGreevy, Solid State Ionics 76 (1995) 301.
[9] R. Tärneberg, Ph.D thesis, University of Gothenburg, 1996.
[10] R. Tärneberg, A. Lundén, Solid State Ionics 90 (1996) 209.
[11] G. Dharmasena, R. Frech, J. Chem. Phys. 102 (1995) 6941.
[12] E.A. Secco, Phys. Status Solidi 88 (1985) 103.
[13] U.M. Gundusharma, C. MacLean, E.A. Secco, Solid State Commun. 57 (1986) 479.
[14] E.A. Secco, J. Solid State Chem. 96 (1992) 366.
[15] E.A. Secco, Solid State Ionics 60 (1993) 233.
[16] T. Kanashiro, T. Yamanishi, Y. Kishimoto, T. Ohno, Y. Michihiro, K. Nobugai, J. Phys. Soc. Jpn. 63 (1994) 3488.
[17] M. Ferrario, M.L. Klein, I.R. McDonald, Mol. Phys. 86 (4) (1995) 923.
[18] C. Pistorius, J. Phys. Chem. Solids 28 (1967) 1811.
[19] C. Pistorius, Z. Phys. Chem. (Neue Folge) 28 (1961) 262.
[20] C. Pistorius, J. Chem. Phys. 43 (8) (1965) 2895.
[21] T. Sakuntala, A.K. Arora, J. Phys. Chem. Solids 61 (2000) 103.
[22] P.T.C. Freire, O. Pilla, V. Lemos, F.E.A. Melo, I. Guedes, J. Mendes Filho, Rev. High Pressure Sci. Technol. 7 (1998) 137.
[23] V.E. Bean, in: G.N. Peggs (Ed.), High Pressure Measurements. Applied Science Publ., London, 1983, p. 93.
[24] S.R. Bohlen, N. Jb. Miner. Mh. H 9 (1984) 404.
[25] R.S. Carmichael, Handbook of Physical Properties of Rocks. CRC Press, Boca Raton, 1966, p. 238.
[26] S. Prabaharan, P. Muthusubramanian, M.A. Kulandainathan, V. Kapali, J. Solid State Chem. 106 (1995) 219.
[27] A.C. Lasaga, Kinetics in the Earth Sciences. Princeton Univ. Press, Princeton, 1997, p. 812.
[28] R.A. Secco, E.A. Secco, J. Phys. Chem. Solids 53 (6) (1992) 749.
[29] R. Secco, Personal communications.
[30] A.R. West, D.C. Sinclair, N. Hirose, J. Electroceram. 1 (1) (1997) 65.
[31] A.K. Jonscher, J. Phys. D: Appl. Phys. 32 (1999) R57.
[32] S.H. Liu, Phys. Rev. Lett. 55 (1985) 529.
[33] R. Frech, D. Teeters, J. Phys. Chem. 88 (1984) 417.
[34] E.K.H. Salje, Phase Transitions in Ferroelastic and Co-elastic Crystals. Cambridge Univ. Press, Cambridge, 1990.
[35] H.C. Freiheit, Order parameter behaviour and thermal hysteresis at the phase transition in the superionic conductor lithium sodium sulfate, $LiNaSO_4$, Solid State Commun., to be submitted.
[36] M. Dove, Am. Mineral. 82 (1997) 213.